Application of first principles based stochastic simulation of surface kinetics for Thiophene Electrohydrogenation

Rajat Daga[1], Kaida Liu[1], Yu Kawamata[2], Phil S. Baran[2], and Matthew Neurock[1]*

[1] Department of Chemical Engineering and Materials Science, University of Minnesota, Minneapolis, Minnesota 55455, US

[2] Department of Chemistry, The Scripps Research Institute, 10550 North Torrey Pines Road, La Jolla, California 92037, United States

*Corresponding author: mneurock@umn.edu

Abstract:

Kinetic Monte Carlo simulations allow us to understand and predict the time evolution of stochastic non-linear processes at the atomic and molecular scale by incorporating lateral interactions and local surface coverage effects. This study presents a generalized C++ object-oriented KMC program, DynKMC, with the capability to model chemical reaction systems with periodic oscillation of a reaction parameter like applied potential. DynKMC incorporates algorithmic acceleration schemes to reduce the computational cost for multi-scale systems. DynKMC is then utilized to study electroreduction of methyl 2-thiophenecarboxylate on reticulated vitreous carbon (RVC) electrode using direct current approach and the novel rapid Alternating Polarity (rAP) approach. KMC simulations, aided with DFT calculations, provide mechanistic reasons for the experimentally observed increase in product selectivity from approximately ~5% using direct current to ~77% using the rAP method. The KMC simulations suggest that alternating potential induces higher surface coverage of thiophene species on the RVC surface, which suppresses the hydrogen evolution reaction (HER) and enhances the product selectivity. Degree of rate control (DRC) calculations suggest that the rate determining step shifts from reactant adsorption in direct current (DC) case to the 2nd hydrogenation step under rAP, suggesting a change in the operating kinetic regime. Additional KMC studies to understand the influence of oscillation time period suggest that increasing the rAP oscillation frequency increases the selectivity of the desired product.

***Keywords**: Kinetic Monte Carlo simulations, Dynamic oscillation, Electroreduction*

Introduction:

Kinetic Monte Carlo (KMC) simulations serve as a versatile kinetic modeling tool extensively employed to model stochastic processes across various scientific and engineering disciplines [6]. The inherent stochasticity and non-linearity of processes, particularly in chemical reaction systems, limits the applicability of deterministic models such as mean-field microkinetic modeling over large variable spaces [1, 2, 3, 4]. Mean-field models do not consider the effect of local surface interactions and surface heterogeneity in heterogeneous reaction systems [7, 8]. While lumped

models considers the effect of average surface coverage on kinetic and energetic parameters [9, 10], they do not account for configuration-dependent effects such as the islanding effects observed in the CO oxidation reaction on the Pt (111) surface [11]. In addition, previous studies have demonstrated that mean-field microkinetic models are prone to statistical errors due to incorrect site pair counting, further restricting the applicability of the mean-field methods [5].

KMC simulations inherently consider surface heterogeneity, as well as the binding orientation and adsorbate configurations, which play a crucial role in determining the surface coverage and lateral interactions [12]. Reaction systems involving aromatic molecules, such as benzene and thiophene, typically block multiple surface sites, rendering single-site occupation models inadequate. Considering multiple adjacent sites, lateral adsorbate interactions, and surface heterogeneity further increases the complexity of mean-field models, making them challenging to solve. A significant limitation limiting the applicability of KMC simulations is their intractable computational cost in a multi-scale system [14, 15]. While previous generalized KMC program accelerates the simulations using GPU cores and parallelization, they do not incorporate algorithmic acceleration schemes which can rescale the fast reactions and enable more frequent execution of the kinetically relevant steps. Previous literature incorporating algorithmic KMC acceleration schemes have been applied to specific systems but have not been integrated as part of generalized KMC program making them difficult to implement for other systems. Therefore, we present a generalized KMC program, DynKMC, integrating algorithmic acceleration schemes to simulate the kinetically relevant steps in multi-scale systems.

DynKMC is applied to the electroreduction of methyl 2-thiophenecarboxylate on an RVC electrode surface [23]. Experiments report <5% selectivity with direct current under -2V vs. SHE and ~77% selectivity under rapid alternating polarity (rAP) between -2V vs. SHE and +2V vs. SHE using periodic square wave oscillation function with a period of 50ms. Due to the inability of experiments to probe reaction variables like surface coverages in real time, the mechanistic reason behind the enhanced selectivity under rAP case remains unclear. Therefore, KMC simulations using DynKMC are employed to understand the differences in reaction variables under DC and rAP conditions to unravel the underlying mechanistic insights for the observed selectivity enhancement under the rAP case. It is shown that rAP enhances the surface coverage of thiophene intermediates, resulting in suppression of hydrogen evolution reaction and therefore enhancing the product selectivity. Simulations are also performed by varying the time period of oscillations to understand the effect of oscillation time period on product selectivity. Degree of rate control (DRC) study is also done using KMC simulations to understand the change in kinetic regime upon transitioning from DC to rAP conditions.

Kinetic Monte Carlo Background:

The traditional KMC algorithm or stochastic simulation algorithm (SSA) is an event-driven simulation where the system evolves by a sequence of discrete reaction events. In the algorithm, a list of all the possible reactions based on the surface configuration is created in an event list. Based on the reaction rate for each event, the cumulative probability for each event is assigned. A random number α is selected from a uniform distribution in the range [0, 1]. An event j is selected from the event list such that α lies between the cumulative probability of event j and event j+1. Another random number β is selected from a uniform distribution in the range [0, 1] to calculate the time increment (Δt_n) in the system clock using the equation *(1)*.

$$\Delta t_n = -\frac{log(\beta)}{\sum_j k_j} \quad (1)$$

While the SSA algorithm accurately solves the CME system of equations, the computational cost of SSA tends to be very high, especially for multi-scale chemical reaction networks. This is due to the high forward and backward reaction rates of the fast equilibrated steps, which results in a high probability for the fast equilibrated steps. This diverts most of the computational effort in simulating the kinetically irrelevant fast equilibrated steps. Therefore, temporal acceleration schemes are required to reduce the computational cost of the SSA algorithm.

This work utilizes a combination of two acceleration schemes, Neurock-Donghai [25] and Neurock-Dybeck [26] acceleration schemes. The Neurock-Donghai scheme involves the categorization of the reactions based on the reaction rates and reversibility into two channels – fast equilibrated and slow or unequilibrated reactions by the user. A fixed number of simulations of the fast reactions specified by the user, are executed on the surface to allow them to equilibrate. Upon equilibration of the fast reactions, a slow or unequilibrated reaction is selected from the event list using the above-mentioned SSA. This ensures the execution of slow steps, while maintaining the surface equilibrated with the fast steps and thereby reducing the computational cost of the simulation. However, this algorithm does not recategorize the reactions within the same channel, which increases the computational cost.

Therefore, the Neurock-Dybeck algorithm is combined with the above approach to circumvent this problem. It is based on the Superbasin approach, which divides the configuration space into superbasins. A superbasin is defined as the set of all configurations that can exist between the execution of two slow unequilibrated reactions. The reactions are divided into equilibrated, quasi-equilibrated, and unequilibrated reactions based on the total number of occurrences and the number of occurrences of the forward and backward steps in a superbasin. The algorithm rescales all the equilibrated reactions to the scale of the fastest quasi-equilibrated or unequilibrated reaction for the execution of the slow reactions within the simulation. This combined algorithm in the DynKMC program allows the user to categorize the reactions prior to the simulation, automatize the categorization of events as fast and slow, and execute the kinetically relevant steps during the KMC simulation. The schematic flowchart of the algorithm is shown in **Figure 1**.

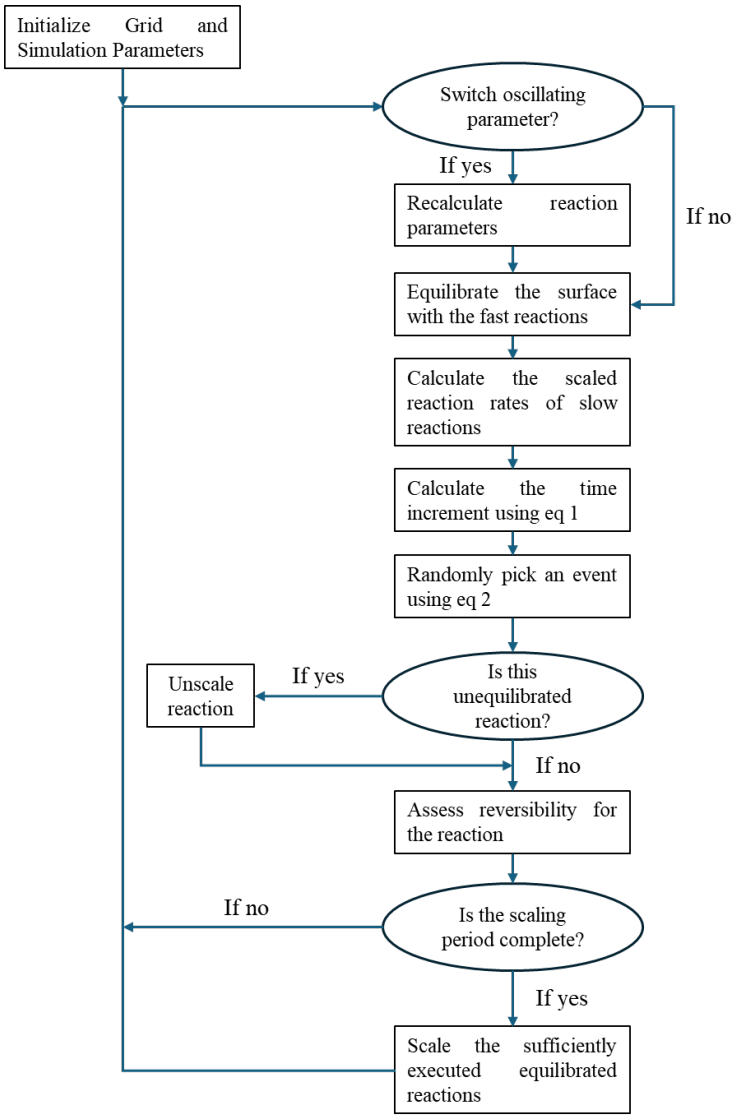

Figure 1: Schematic flowchart of the KMC program with combined acceleration scheme and oscillating reaction conditions

The outline for the KMC algorithm implemented in the DynKMC program is presented below. The algorithm is depicted schematically in Figure 1.

1. Generate an initial surface configuration (δ) (t = 0)
2. Initialize the kinetic and interaction parameters
3. Equilibrate the surface with the fast elementary steps set by the user using the Donghai approach [25] and update the surface configuration (γ).
4. Determine the reaction rate ($r_{\gamma\beta}$) for all the slow elementary steps taking surface configuration from γ to a surface configuration β and calculate the total reaction rate as

$$r_{tot(\gamma)} = \sum_{\beta} r_{\gamma\beta}. \qquad (2)$$

5. Select the elementary step i taking the surface configuration from $\gamma \rightarrow \gamma'$ such that the following inequality holds:

$$\sum_{\beta<\gamma'-1} r_{\gamma\beta} < \rho_1 \times r_{tot(\gamma)} \leq \sum_{\beta<\gamma'} r_{\gamma\beta} \quad (3)$$

where ρ_1 is a randomly generated number from a uniform distribution in the interval [0,1].

6. Advance the time using a second random number using the equation *(4)*:

$$t = t - \frac{\ln \rho_2}{r_{tot(\gamma)}} \quad (4)$$

where ρ_2 is a randomly generated number from a uniform distribution in the interval [0,1].

7. Calculate the equilibration ratio (*e*) of the selected step using equation (**5**). If the ratio is within the tolerance specified by the user, mark the step as equilibrated.

$$\boldsymbol{e = \frac{N_f - N_b}{N_f}} \quad (5)$$

where N_f and N_b is the number of forward and backward steps respectively recorded in the current superbasin

8. If the selected step is equilibrated and has been executed more than the user specified frequency in the current superbasin, rescale the preexponential factor of both forward and reverse step using the scaling factor (α) in equation (**6**),

$$\boldsymbol{\alpha = \frac{r_{max,avg}}{\left(\frac{r_{f,i} + r_{b,i}}{2}\right)}}. \quad (6)$$

where $r_{max,avg}$ is the maximum rate among unequilibrated steps averaged over time in the current superbasin, $r_{f,i}$ is the averaged rate over time of the forward selected step and $r_{b,i}$ is the averaged rate over time of the backward selected step. The time-averaged rate of the elementary step *i* ($\boldsymbol{r_i}$) is calculated using the equation (7).

$$\boldsymbol{r_i = \frac{1}{\Delta t_s} \sum_j r_{i,j} \Delta t_j} \quad (7)$$

where $\boldsymbol{\Delta t_s}$ is the time spent in the superbasin, $\boldsymbol{\Delta t_j}$ is the time step of each KMC step j and $r_{i,j}$ is the rate of elementary step *i* at KMC step j.

9. If the selected step is an unequilibrated step, rescale the scaling factor (α) of all the slow steps specified by the user to 1.
10. Update the system configuration from γ to γ'
11. Check whether the end criterion is reached. If yes, then end the simulation. Otherwise continue to step 12.
12. Check whether the time increment results in changing the oscillation parameter. If yes, update the oscillation parameter and go to step 2. Otherwise go to step 3.

On-the-fly calculation of interatomic interaction energy in DynKMC program is executed through two different pathways – "Through space" and "Through surface" interactions. "Through space" interaction is accounted using Merck molecular force field (MMFF94) [27] non-bonding interaction terms – van der Waals and electrostatic interaction terms. "Through surface" interaction involves the interaction between adsorbates due to metal atom sharing. This interaction is calculated using the unity bond index – quasi exponential potential (UBI-QEP) theory [28], based

on the bond order conservation (BOC) principle. The DynKMC program considers the heterogeneity of the surface by explicitly considering the atop, bridge, 3-fold hollow, and 4-fold hollow sites. In addition, the program can define 2D square planar (100), hexagonal (111) metal surfaces, and graphene-type surfaces to model the reticulated vitreous carbon (RVC) or graphene surface.

Case Study: Thiophene Electroreduction on Graphene electrode

The above presented DynKMC program is demonstrated by its application to methyl 2-thiophenecarboxylate electroreduction reaction. The electroreduction of methyl 2-thiophenecarboxylate (**a**) is hypothesized to take place through the Electrochemical Chemical Electrochemical Chemical (ECEC) pathway on the RVC electrode using DFT calculations [Kaida's Work], as shown in **Figure 1**. The ECEC mechanism involves the adsorption of reactant **a** followed by electron transfer from the surface to the molecule resulting in the formation of a negatively charged radical **b**. A proton transfer step takes place from the hydrogenated ethanol to the radical intermediate to form a neutral radical molecule **c**. Another electron is transferred from the electrode resulting in a negatively charged radical **d** which is protonated by a hydrogenated ethanol molecule, resulting in the formation of product **e**.

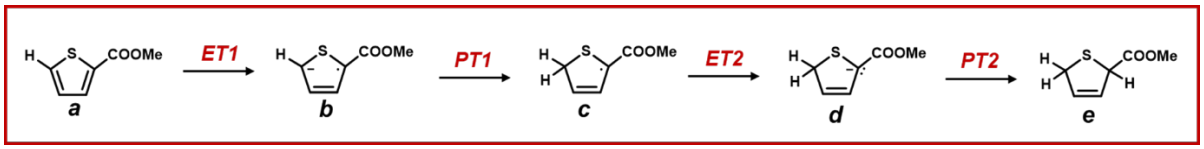

Figure 2: The Electrochemical Chemical Electrochemical Chemical (ECEC) pathway as described in the DFT calculations

At a reducing potential of -2V vs. the Standard Hydrogen Electrode (SHE), the primary side reaction occurring on the RVC electrode is the Hydrogen Evolution Reaction (HER). This reaction proceeds via the Volmer-Heyrovský mechanism, as supported by previous Density Functional Theory (DFT) calculations [Kaida's work].

In the initial Volmer step, a protonated ethanol molecule ($C_2H_5OH_2^+$) is attracted to the negatively charged electrode surface, occupying the surface site. The protonated ethanol then dissociates to form an H* adsorbate on the surface and an ethanol molecule in the bulk solvent. The Volmer step can be expressed as follows:

$$C_2H_5OH_2^+ + e^- + * \rightarrow H* + C_2H_5OH$$

Subsequently, in the Heyrovský step, another protonated ethanol molecule approaches the adsorbed hydrogen atom, resulting in the formation of ethanol and the evolution of molecular hydrogen. The Heyrovský step can be expressed as follows:

$$C_2H_5OH_2^+ + e^- + H* \rightarrow H_2 + C_2H_5OH + *$$

Kinetics used in Kinetic Monte Carlo simulations

Table 1: Kinetics of thiophene hydrogenation at +2V vs. SHE potential (blue) and -2V vs. SHE potential (red)

Reaction Number	Forward Preexp (s^{-1})		Forward Barrier (kJ/mol)		Reaction	Backward Preexp (s^{-1})		Backward Barrier (kJ/mol)	
1	-	10^6	-	28	$C_2H_5OH_2^+ + e^- + * = C_2H_5OH_2*$	10^{13}	10^{13}	45	128
2	10^{13}	10^{13}	25	25	$C_2H_5OH_2* = C_2H_5OH + H*$	10^7	10^8	185	180
3	10^6	10^6	65	25	$C_2H_5OH_2^+ + e^- + H* = H_2 + C_2H_5OH + *$	-	-	-	-
4	10^8	10^6	20	25	$C_6H_6O_2S + * = C_6H_6O_2S*$	10^{13}	10^{13}	95	50
5	-	10^{13}	-	0	$C_6H_6O_2S* + e^- = C_6H_6O_2S^-*$	10^{13}	-	0	-
6	-	10^9	-	35	$C_6H_6O_2S^-* + C_2H_5OH_2^+ = C_2H_5OH + C_6H_7O_2S*$	10^8	10^8	75	65
7	-	10^{13}	-	0	$C_6H_7O_2S* + e^- = C_6H_7O_2S^-*$	10^{13}	-	0	-
8	-	10^9	-	44	$C_6H_7O_2S^-* + C_2H_5OH_2^+ = C_2H_5OH + C_6H_8O_2S*$	10^8	10^8	110	104
9	10^{13}	10^{13}	70	15	$C_6H_8O_2S* = C_6H_8O_2S + *$	10^2	10^2	0	0
10	10^{13}	-	0	-	$H* = H^+ + * + e^-$	-	-	-	-
11	10^6	-	25	-	$C_2H_5OH + * = C_2H_5OH*$	10^{13}	10^{13}	65	35

Table 1 elucidates the kinetics used in the KMC simulation. At +2V vs. SHE, it is assumed that the protons would not be close enough to the surface due to electrostatic repulsion, resulting in no adsorption of the protonated ethanol. Also, the H* adsorbed on the surface is readily oxidized to form a proton and reacts with ethanol and exists as protonated ethanol in the solution. The positive surface charge would attract the nucleophile sulfur atom closer to the surface in the EDL, resulting in more frequent collisions and therefore higher preexponential factor. Also, it is assumed that the barrier for thiophene adsorption reduces by 5kJ/mol due to attractive electrostatic attractions.

At -2V vs. SHE, the protonated ethanol comes closer to the surface due to favorable electrostatic interactions resulting in high preexponential factor. The negative surface charge favors the adsorption of H* on the surface, resulting in higher H* surface coverage. It is assumed that the negatively charged intermediates do not transfer the negative charge to the surface at -2V vs. SHE. The negative surface charge repels the thiophene species resulting in lower adsorption energy and lower preexponential factor for thiophene adsorption.

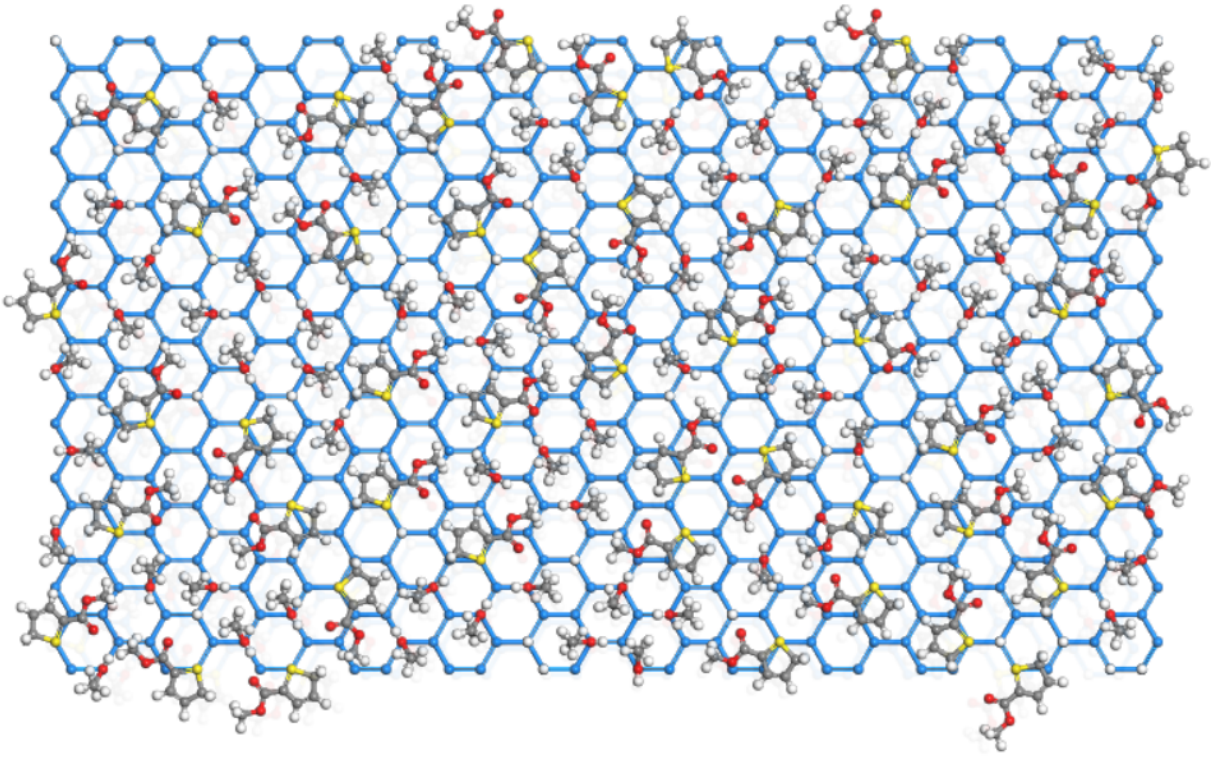

Figure 3: The snapshot of surface from kMC simulation under constant -2V vs. SHE. The blue atoms represent graphene surface, red atoms oxygen, white atoms hydrogen and yellow atoms sulfur and gray atoms carbon

KMC simulations for the DC case yield a product selectivity of ~8%, which is close to the experimentally observed value (<5%) [23]. The remainder of the product is H_2 produced through HER. Error! Reference source not found.Error! Reference source not found.**a** shows the snapshot of a working catalyst surface under -2V vs. SHE from the KMC simulations. It can be observed from the snapshot that the surface is sparsely populated by thiophene molecules due to weak thiophene adsorption energy. The remaining sites are occupied by H* through the Volmer step and the protonated ethanol (solvent) molecules. **Figure 6a** shows the plot of surface coverage with time. It can be observed that the surface coverages of thiophene species, H* and protonated ethanol are ~0.2ML. Since the rate constant for HER is higher than the desired pathway at -2V vs. SHE, HER is the dominant reaction taking place on the surface. This results in low selectivity and yield for product molecule **e**. Therefore, HER suppression is important to enhance the selectivity of the desired product.

Baran et.al., shows that rAP suppresses HER through periodic oscillation between positive (+2V vs. SHE) and negative (-2V vs. SHE) potentials. Error! Reference source not found.**b** shows the snapshot of the model of a working catalyst surface under +2V vs. SHE regime in the rAP case. Under +2V vs. SHE, the binding energy of reactant **a** is stronger due to the favorable electrostatic interaction of the electron-rich sulfur atom in reactant **a** and the positively charged surface. In addition, the H* adsorbates on the surface oxidize and desorb as protonated ethanol, resulting in higher equilibrium surface coverage of thiophene species and negligible H* surface coverage compared to -2V vs. SHE, as shown in the surface coverage vs. time plot in **Figure 6b**.

However, no further reduction of the reactant and intermediate will take place due to the oxidizing potential.

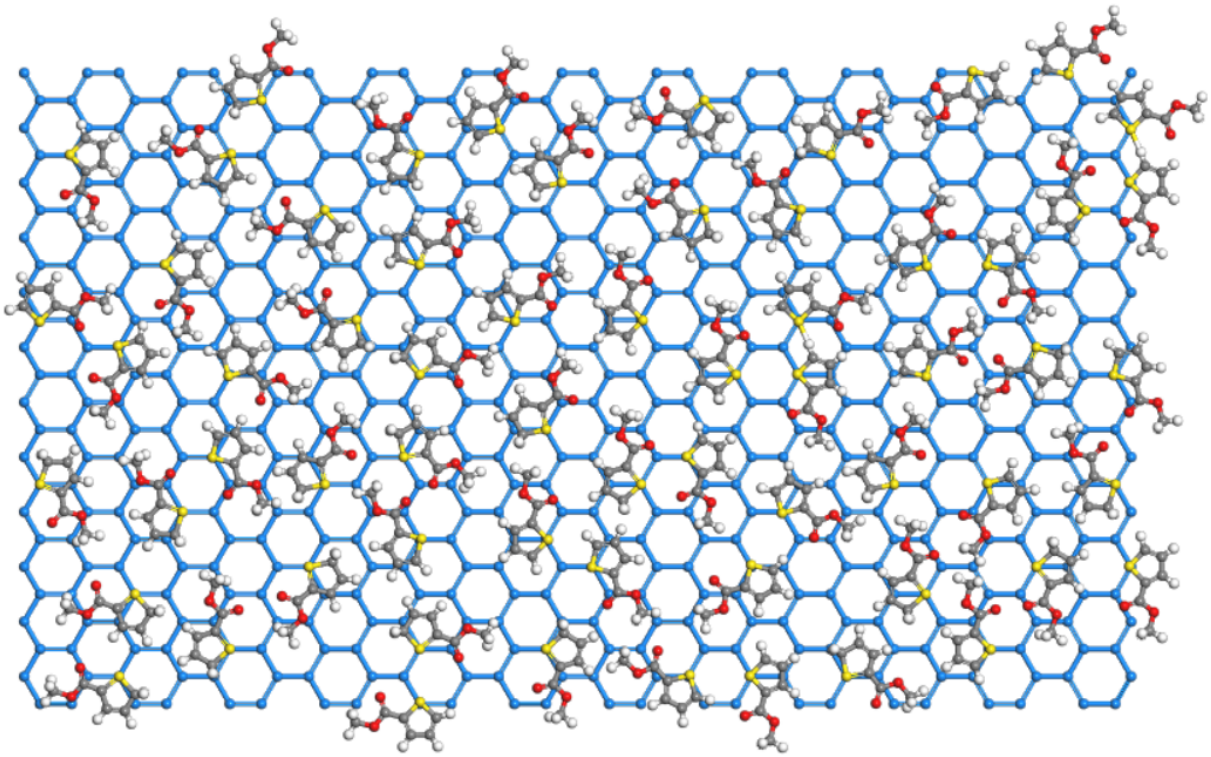

Figure 4: Snapshot of the surface under +2V vs. SHE at rAP conditions. The blue atoms represent graphene surface, red atoms oxygen, white atoms hydrogen and yellow atoms sulfur and gray atoms carbon

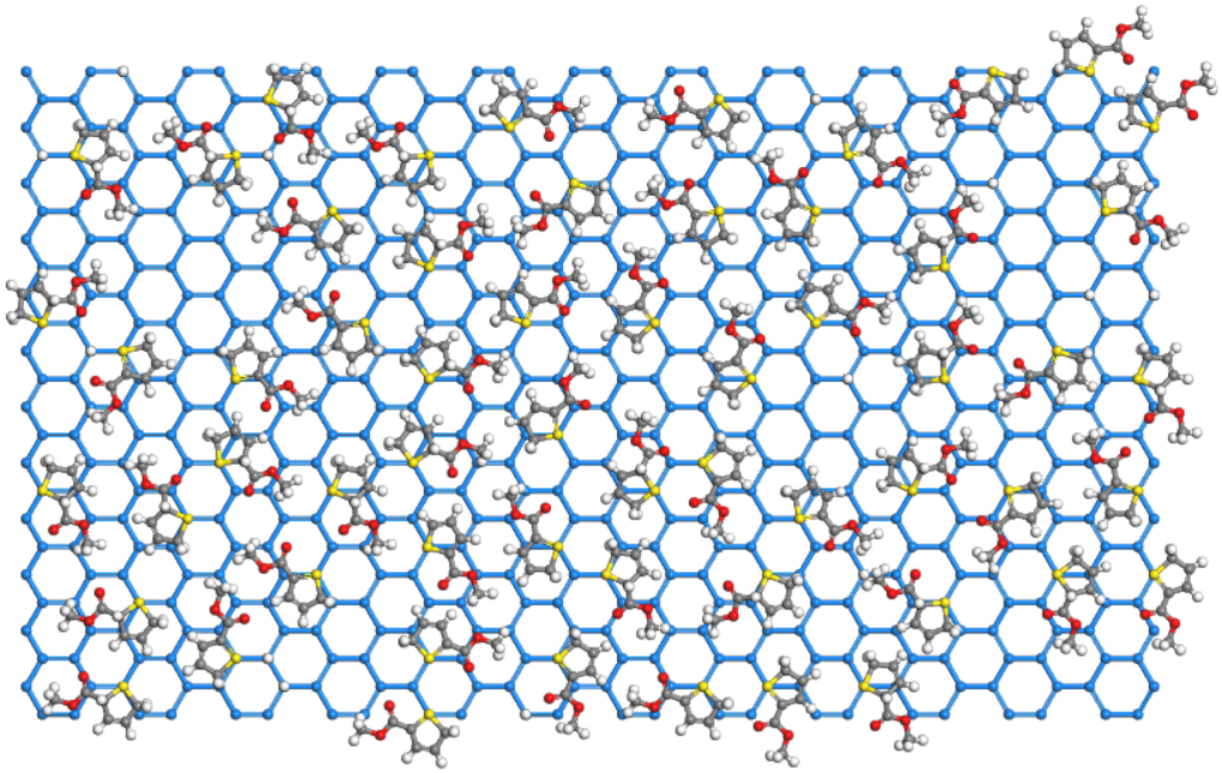

Figure 5: Snapshot of the surface under -2V vs. SHE at rAP conditions. The blue atoms represent graphene surface, red atoms oxygen, white atoms hydrogen and yellow atoms sulfur and gray atoms carbon

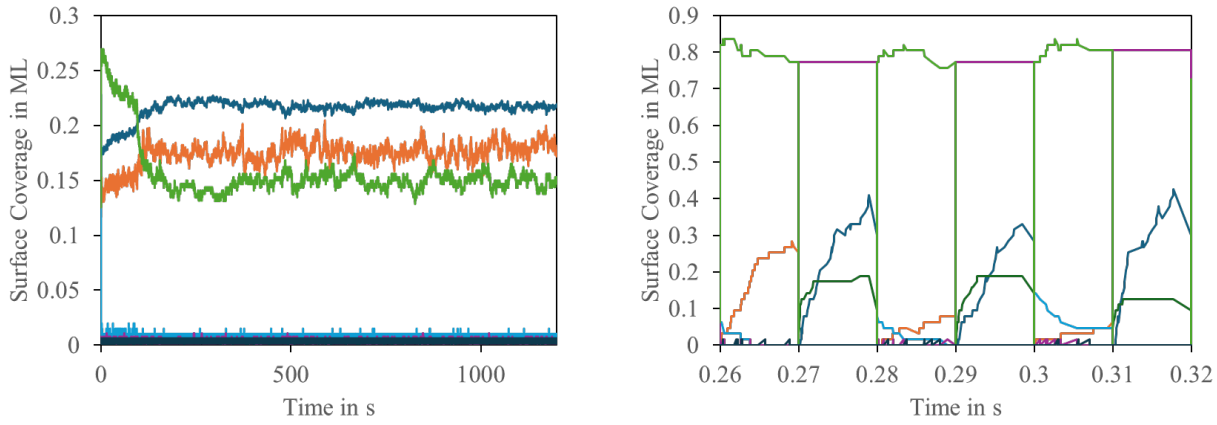

Figure 6: Surface coverage plot of the species as a function of time for (a) DC case (b) rAP case.

Upon alternating the potential to -2V vs. SHE, electrons will be transferred to the adsorbate species resulting in the formation of reaction intermediates and subsequently product through hydrogenation. Error! Reference source not found.**c** is a snapshot of the model of a working catalyst surface under -2V vs. SHE regime in the rAP case. Due to the repulsive interaction between the lone pair electrons of sulfur on thiophene and the negatively charged surface, the binding strength at -2V vs. SHE is weaker, resulting in easy desorption of the product molecules from the surface. This leads to the formation of desired product molecules in the solution and vacant sites on the surface, as shown in the surface coverage vs. time plot in **Figure 6b**. Switching

back to +2V vs. SHE would result in the adsorption of reactant **a** at the vacant sites, reducing the H* surface coverage.

KMC simulations under the rAP case predict enhancement in the product selectivity to >70%, increasing from 8% in the DC case. At an oscillation frequency of 20Hz, the KMC predicted selectivity of 77% correlates well with the experimentally observed selectivity of 83% [23]. KMC simulations suggest that the most abundant surface intermediate (MASI) under the rAP case is the intermediate **b** species, with a very small surface coverage of H* species. Low surface coverage of H* results in the suppression of HER.

Despite the sites being blocked by thiophene adsorption, a small fraction of HER is still observed under rAP conditions. This is because the product desorbs readily at -2V vs. SHE, leaving behind vacant sites. Species **a** and protonated ethanol compete for adsorption on these vacant sites. Since adsorption of protonated ethanol and subsequently HER is favored at -2V vs. SHE, H_2 evolves from the surface resulting in incomplete suppression of HER.

Effect of time period on the thiophene electroreduction

Figure 7 shows the effect of time period on the selectivity and yield of the product. The error bars in the figure are obtained by running multiple KMC simulations using 10 different seeds for the random number generator given in SI. A time period of 100ms results in 50% selectivity. At longer time periods, the selectivity will further decrease until it reaches ~8%, which is the observed selectivity under the DC case. The selectivity increases to ~96% upon further reducing the time period to 10ms. It can be observed that the selectivity increases monotonically with time period. This trend of selectivity with changing time period is expected since the desorption of the product molecules at -2V vs. SHE results in the formation of vacant sites. HER and the adsorption of reactant **a** compete on the vacant sites. Due to higher rates of HER, HER dominates on the vacant site resulting in lower product selectivity with higher time periods.

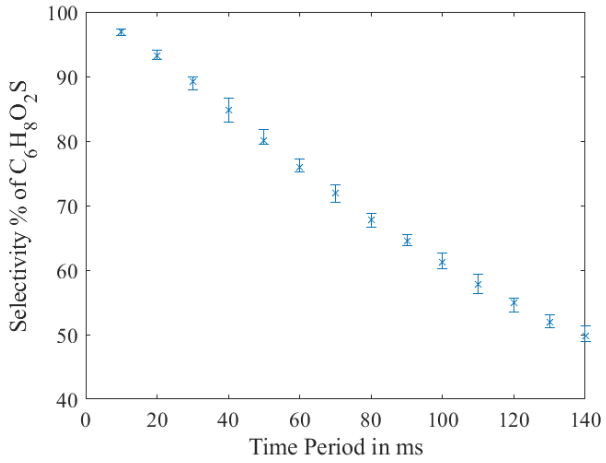

Figure 7: The plot of selectivity % as a function of time period using KMC simulations

Effect of rAP on the rate determining step using Degree of Rate Control (DRC) calculation

Degree of Rate Control (DRC) for elementary step i is defined as the change in the natural log of overall reaction rate per relative increase in the natural log of the rate constant for the step i, holding all the equilibrium constants, K_i for step i, and the forward and reverse rate constants for step $j \neq i$ [30]. It is mathematically given by the following equation:

$$X_{RC,i} = \frac{k_i}{r}\frac{\partial r}{\partial k_i}\Big|_{k_{j,j\neq i}K_j,} = \frac{\partial lnr}{\partial lnk_i}\Big|_{k_{j,j\neq i}K_j,} \quad (8)$$

To identify the rate limiting step and quantify the effect of rAP on the rate limiting step, the DRC for each of the kinetically relevant elementary steps is calculated and shown in **The DRC** values for the adsorption step of reactant **a** and the 2nd hydrogenation step under DC and rAP case are shown in **Table 2.** Under the DC case, the DRC of the adsorption step of reactant **a** is the highest. This is because the reaction is limited by the low surface coverage of the reactant thiophene species and high H* surface coverage resulting in high HER rates and low rates of the desired mechanism. rAP results in an enhancement of the thiophene species surface coverage due to stronger adsorption of reactant **a** and the oxidation of H* to proton at +2V vs. SHE. This results in reduction of the DRC value of the adsorption step of reactant **a**. The rate controlling step then shifts to the next kinetically most relevant step, 2nd hydrogenation step, signified by the maximum DRC value under rAP. Therefore, to further increase the rate under rAP conditions, reaction conditions which favor the 2nd hydrogenation step should be utilized.

Table 2. To calculate the DRC in the KMC simulations, the activation barrier of the elementary steps is perturbed to understand the change in the rate of the overall reaction with respect to the activation barriers. Using the Arrhenius equation for the rate constant, the DRC equation can be rewritten as:

$$X_{RC,i} = -RT\frac{\partial lnr}{\partial E_A}\Big|_{k_{j,j\neq i},K_j} \quad (9)$$

The DRC values for the adsorption step of reactant **a** and the 2nd hydrogenation step under DC and rAP case are shown in **Table 2**. Under the DC case, the DRC of the adsorption step of reactant **a** is the highest. This is because the reaction is limited by the low surface coverage of the reactant thiophene species and high H* surface coverage resulting in high HER rates and low rates of the desired mechanism. rAP results in an enhancement of the thiophene species surface coverage due to stronger adsorption of reactant **a** and the oxidation of H* to proton at +2V vs. SHE. This results in reduction of the DRC value of the adsorption step of reactant **a**. The rate controlling step then shifts to the next kinetically most relevant step, 2nd hydrogenation step, signified by the maximum DRC value under rAP. Therefore, to further increase the rate under rAP conditions, reaction conditions which favor the 2nd hydrogenation step should be utilized.

Table 2: DRC values for the kinetically relevant elementary steps under DC and rAP conditions

Reaction	X_{RC} under DC	X_{RC} under rAP
Thiophene adsorption	**0.7**	0.13
2nd hydrogenation step	0.27	**0.75**

Future Direction

While KMC simulations elucidate the role of surface coverage in enhancing the selectivity of product molecules under rAP conditions, they assume that mass transfer rate of the reactants from the bulk solution to the surface is higher than the reaction rates resulting in insignificant time spent for the formation and destruction of electric double layer (EDL). If the timescales for EDL formation and solvent equilibration are comparable to the rAP oscillation period, the system may become mass transfer limited rather than reaction limited. Baran's group conducted an optimization study on the electroreduction of ethyl hippurate using rAP [23], finding that although selectivity increased with a decreasing oscillation period, the faradaic efficiency decreased when the period fell below 50ms. This leads to a peak faradaic efficiency around 50ms, attributed to the matching timescales of EDL formation with the oscillation period, causing mass transfer to become the rate-controlling step.

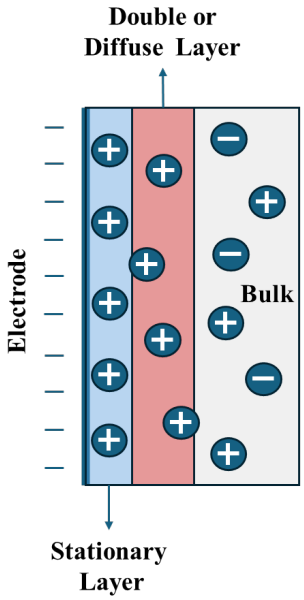

Figure 8: A diagram of the different layers in the solution phase under cathodic conditions

Currently, the DynKMC program models the atomic processes on the catalyst surface and does not consider the effect of dynamic applied potential oscillation on the concentration in the EDL. To account for concentration differences due to double layer formation, KMC simulations must be coupled with models that accurately depict these concentration changes in the EDL. One method to account for concentration changes is using continuum models [31]. Although continuum models can be integrated with the KMC program, estimating the diffusion parameters due to electrostatic interactions remains challenging. Conversely, Molecular Dynamics (MD) simulations can more accurately model the time evolution of compound concentrations in the solution layer but are computationally intensive and difficult to integrate with KMC. A viable approach would involve training the continuum model using MD simulations and then integrating this continuum model with the KMC simulations. Therefore, future development of the KMC program for electrochemical systems should focus on incorporating MD simulations through continuum modeling within the KMC framework to account for concentration variations in the EDL due to rAP.

References

[1] S. Matera, H. Meskine and K. Reuter, "Adlayer inhomogeneity without lateral interactions: Rationalizing correlation effects in CO oxidation at RuO2 (110) with first-principles kinetic Monte Carlo.," *The Journal of chemical physics,* vol. 134, no. 6, 2011.

[2] B. Temel, H. Meskine, K. Reuter, M. Scheffler and H. Metiu, "Does phenomenological kinetics provide an adequate description of heterogeneous catalytic reactions?," *The Journal of chemical physics,* vol. 126, no. 20, 2007.

[3] Z. Chen, H. Wang, N. Su, S. Duan, T. Shen and X. Xu, "Beyond mean-field microkinetics: toward accurate and efficient theoretical modeling in heterogeneous catalysis," *ACS Catalysis,* vol. 8, no. 7, pp. 5816-5826, 2018.

[4] H. Prats, F. Illas and R. Sayos, "General concepts, assumptions, drawbacks, and misuses in kinetic m onte c arlo and microkinetic modeling simulations applied to computational heterogeneous catalysis.," *International Journal of Quantum Chemistry,* vol. 11, 2018.

[5] N. Razdan and A. Bhan, "Catalytic site ensembles: A context to reexamine the Langmuir-Hinshelwood kinetic description.," *Journal of Catalysis,* vol. 404, pp. 726-744, 2021.

[6] D. Gillespie, "A general method for numerically simulating the stochastic time evolution of coupled chemical reactions.," *Journal of computational physics,* vol. 22, no. 4, pp. 403-434, 1976.

[7] M. Andersen, C. Plaisance and K. Reuter, "Assessment of mean-field microkinetic models for CO methanation on stepped metal surfaces using accelerated kinetic Monte Carlo.," *The Journal of chemical physics,* vol. 147, no. 15, 2017.

[8] M. Pineda and M. Stamatakis, "Beyond mean-field approximations for accurate and computationally efficient models of on-lattice chemical kinetics.," *The Journal of Chemical Physics,* vol. 147, no. 2, 2017.

[9] T. Mou, X. Han, H. Zhu and H. Xin, "Machine learning of lateral adsorbate interactions in surface reaction kinetics.," *Current Opinion in Chemical Engineering,* vol. 36, p. 100825, 2022.

[10] W. Xie, J. Xu, J. Chen, H. Wang and P. Hu, "Achieving theory–experiment parity for activity and selectivity in heterogeneous catalysis using microkinetic modeling.," *Accounts of Chemical Research,* vol. 55, no. 9, pp. 1237-1248, 2022.

[11] S. Akhter and J. White, "The effect of oxygen islanding on Co and H2 oxidation on Pt (111).," *Surface science,* vol. 171, no. 3, pp. 527-542, 1986.

[12] L. Danielson, M. Dresser, E. Donaldson and J. Dickinson, "Adsorption and desorption of ammonia, hydrogen, and nitrogen on ruthenium (0001)," *Surface Science,* vol. 71, no. 3, pp. 599-614, 1978.

[13] A. Jansen, An introduction to kinetic Monte Carlo simulations of surface reactions (Vol. 856)., Springer, 2012.

[14] M. Pineda and M. Stamatakis, "Kinetic Monte Carlo simulations for heterogeneous catalysis: Fundamentals, current status, and challenges.," *The Journal of Chemical Physics,* vol. 156, no. 12, 2022.

[15] H. Gao, L. Oakley, I. Konstantinov, S. Arturo and L. Broadbelt, "Acceleration of kinetic Monte Carlo method for the simulation of free radical copolymerization through scaling.," *Industrial & Engineering Chemistry Research,* vol. 54, no. 48, p. 1197, 2015.

[16] C. Lim, M. Hülsey and N. Yan, "Non-faradaic promotion of ethylene hydrogenation under oscillating potentials.," *JACS Au,* vol. 1, no. 5, pp. 536-542, 2021.

[17] K. Fraysse, S. Meaney, W. Gates, D. Langley, R. Tabor, P. Stoddart and G. Greene, "Frequency Dependent Silica Dissolution Rate Enhancement under Oscillating Pressure via an Electrochemical Pressure Solution-like, Surface Resonance Mechanism.," *Journal of the American Chemical Society,* vol. 144, no. 9, pp. 3875-3891, 2022.

[18] J. B. A. R. C. H. A. Timoshenko, R. Arán-Ais, H. Jeon, F. Haase, U. Hejral, P. Grosse, S. Kühl and E. Davis, "Steering the structure and selectivity of CO2 electroreduction catalysts by potential pulses.," *Nature catalysis,* vol. 5, no. 4, pp. 259-267, 2022.

[19] S. Gathmann, C. Bartel, L. Grabow, O. Abdelrahman, C. Frisbie and P. Dauenhauer, "Dynamic Promotion of the Oxygen Evolution Reaction via Programmable Metal Oxides," *ACS Energy Letters,* vol. 9, no. 5, pp. 2013-2023, 2024.

[20] V. Vempatti, S. Wang, O. Abdelrahman, P. Dauenhauer and L. Grabow, "Catalytic Resonance of Methane Steam Reforming by Dynamically Applied Charges," 2024.

[21] E. Hansen, Methodology for stochastic simulations of surface kinetics from first-principles., University of Virginia, 2001.

[22] E. Hansen and M. Neurock, "Modeling surface kinetics with first-principles-based molecular simulation," *Chemical engineering science,* vol. 54, no. 15-16, pp. 3411-3421, 1999.

[23] K. Hayashi, J. Griffin, H. K. C., Y. Kawamata and P. S. Baran, "Chemoselective (hetero) arene electroreduction enabled by rapid alternating polarity.," *Journal of the American Chemical Society,* vol. 144, no. 13, pp. 5762-5768, 2022.

[24] D. Gillespie, "A rigorous derivation of the chemical master equation.," *Physica A: Statistical Mechanics and its Applications,* vol. 188, no. 1-3, pp. 404-425, 1992.

[25] D. Mei, P. Sheth, M. Neurock and C. Smith, "First-principles-based kinetic Monte Carlo simulation of the selective hydrogenation of acetylene over Pd (111)," *Journal of Catalysis,* vol. 242, no. 1, pp. 1-15, 2006.

[26] E. Dybeck, C. Plaisance and M. Neurock, "Generalized temporal acceleration scheme for kinetic monte carlo simulations of surface catalytic processes by scaling the rates of fast reactions.," *Journal of chemical theory and computation,* vol. 13, no. 4, pp. 1525-1538, 2017.

[27] T. Halgren, "Merck molecular force field. II. MMFF94 van der Waals and electrostatic parameters for intermolecular interactions.," *Journal of Computational Chemistry,* vol. 17, no. 5-6, pp. 520-552, 1996.

[28] E. Shustorovich and H. Sellers, "The UBI-QEP method: a practical theoretical approach to understanding chemistry on transition metal surfaces.," *Surface science reports,* vol. 31, no. 1-3, pp. 1-119, 1998.

[29] A. J. Birch, "The Birch reduction in organic synthesis," *Pure and Applied Chemistry,* vol. 68, no. 3, pp. 553-556, 1996.

[30] C. Campbell, "Future directions and industrial perspectives micro-and macro-kinetics: their relationship in heterogeneous catalysis.," *Topics in Catalysis,* vol. 1, pp. 353-366, 1994.

[31] F. Röder, R. Braatz and U. Krewer, "Direct coupling of continuum and kinetic Monte Carlo models for multiscale simulation of electrochemical systems.," *Computers & Chemical Engineering,* vol. 121, pp. 722-735, 2019.

[32] Y. Kawamata, K. Hayashi, E. Carlson, S. Shaji, D. Waldmann, B. Simmons, J. Edwards, C. Zapf, M. Saito and P. Baran, "Chemoselective electrosynthesis using rapid alternating polarity.," *Journal of the American Chemical Society,* vol. 143, no. 40, 2021.

[33] D. Grahame, "The electrical double layer and the theory of electrocapillarity.," *Chemical reviews,* vol. 41, no. 3, pp. 441-501, 1947.